Strong and Tough Physical Eutectogels Regulated by the Spatiotemporal Expression of Non-Covalent Interactions

Hao Zhang, Ning Tang, Xia Yu, Min-Hui Li, Jun Hu

ADVANCED FUNCTIONAL MATERIALS
www.afm-journal.de

Strong and Tough Physical Eutectogels Regulated by the Spatiotemporal Expression of Non-Covalent Interactions

*Hao Zhang, Ning Tang, Xia Yu, Min-Hui Li, and Jun Hu**

Physical eutectogels are appealing materials for technological devices due to their superior ionic conductivity, thermal and electrochemical stability, non-volatility, and low cost. Nevertheless, current physical eutectogels are suffering from weak mechanical strength and toughness. Here, taking advantage of the distribution difference of polyvinyl alcohol (PVA) in water and deep eutectic solvents (DESs), a simple and universal solvent-replacement approach is proposed to regulate the spatiotemporal expression of intra/interpolymer interactions to prepare strong and tough physical eutectogels. The exchange of DESs with water can restrengthen the weakened interactions between PVA chains in water, enabling PVA to crystallize to construct a uniform and robust polymer network. Consequently, the resultant PVA eutectogel exhibits record-high strength (20.2 MPa), toughness (62.7 MJ m^{-3}), and tear-resistance (tearing energy Σ42.4 kJ m^{-2}), while possessing excellent stretchability (Σ550% strain), repairability, and adhesive performance. Furthermore, this strategy is proven to be universally applicable to various species of polymers, and even can be utilized to fabricate continuous and conductive eutectogel fibers, demonstrating potential as engineering materials and wearable sensors.

1. Introduction

The rise of artificial intelligence, and implantable and wearable electronics has led to an ongoing search for synthetic methods of flexible gel materials.[1–7] At present, traditional gels using water, organic solvents, or ionic liquids as continuous phases are facing the problems of poor temperature-resistance, low conductivity, bio-incompatibility, and high cost, realistically impeding their applications.[8–11] Eutectogels, a new class of soft materials that have just emerged in the gel family in recent years, are composed of cross-linked polymer networks and deep eutectic solvents (DESs). Benefiting from the inherent high-electrical conductivity, weak volatility, extensive thermal stability, and low cost of DESs,[12–14] eutectogels are well placed to replace temperature-resistant hydrogels and expensive ionogels as flexible ionic conductors, with immeasurable prospects in energy, electronics, and environmental science.[10,15–18]

Typically, in situ radical polymerization of double-bond monomers in DESs is the most common method for the manufacture of eutectogels.[19–21] But the conversion of monomers to polymers is risky if polymerization is incomplete, which in turn produce biotoxic chemical residues. Moreover, the limited type and the non-biodegradability of monomers prompt a reconsideration of their usage as flexible materials in direct contact with biological systems (e.g., skin).[22] On the contrary, eutectogels using physically interacting polymer networks are often praised for their dynamic recoverability and biosafety, making them a viable alternative to chemical cross-linked gels. However, due to the weak non-covalent interactions, they usually lack adequate stability and mechanical strength.[23] Note that although various techniques such as freezing–thawing,[24] salting out,[25] directional freezing,[26] and annealing[27] have been proved to significantly improve the mechanical performance of physical hydrogels, these strategies are not suitable for physical eutectogels because of the intrinsic differences in the physical and chemical properties between DESs and water. Thus, how to construct strong and tough physical eutectogels remains a big challenge.

As a general rule, flexible gel materials with homogeneous polymer networks and strong polymer–polymer interactions are considered to be effective in dispersing deformation forces and maximizing the synergistic effect of polymer chains, thus showing excellent mechanical strength.[28,29] Accordingly, in order to obtain a strong and tough physical eutectogel, the polymer–polymer interactions should first be weakened so that the polymer can be dissolved in DESs completely and interwoven into a homogeneous network in a free-chain state (this process is referred to as "polymer dissociation"). Following that, in the sol–gel transition process, the broken polymer–polymer interactions can be restored or strengthened to establish a reliable polymeric framework (this process is referred to as "network reconstruction"). During the "polymer dissociation" and "network reconstruction" processes, manipulating the spatiotemporal expression of non-covalent interactions between

H. Zhang, N. Tang, X. Yu, M.-H. Li, J. Hu
Beijing Advanced Innovation Center for Soft Matter Science and Engineering
Beijing University of Chemical Technology
North Third Ring Road 15, Chaoyang, Beijing 100029, China
E-mail: jhu@mail.buct.edu.cn
M.-H. Li
Chimie ParisTech
CNRS
Institut de Recherche de Chimie Paris
PSL University Paris
11 rue Pierre et Marie Curie, Paris 75005, France
The ORCID identification number(s) for the author(s) of this article can be found under https://doi.org/10.1002/adfm.202206305.

DOI: 10.1002/adfm.202206305

polymers is essential to realize the optimization of polymer networks and obtain strong and acceptable eutectogels.

Traditionally, people usually adopt heating–cooling process to regulate the polymer–polymer interactions. But the final properties of materials are not optimal due to the inability to establish a homogenous and robust polymer network.[30] Here for the first time, we describe a simple and universal solvent-replacement approach to develop strong and tough physical eutectogels. Poly(vinyl alcohol) (PVA) is chosen as a representative polymer backbone, as its crystalline domains induced by dense hydrogen bonds can provide an abundance of physical cross-linking sites. This approach involves a two-step process: first, relying on prominent solvent-polymer interactions to disrupt polymer–polymer interactions in good solvent (i.e., water) to form a highly hydrated polymer network, and subsequently, restrengthening the disrupted polymer–polymer interactions by replacing water with DESs (poor solvent) to rebuild a homogeneous, robust polymer network. In contrast to the traditional method of constructing eutectogels directly in DESs, the solvent-replacement process is a well-controlled approach that can regulate the spatiotemporal expression of polymer–polymer interactions for achieving the optimization of "polymer dissociation" and "network reconstruction". Our as-prepared PVA eutectogels (DESs-PVA) demonstrate ultrahigh ultimate stress (i.e., 20.2 MPa), toughness (i.e., 62.7 MJ m^{-3}), and tearing energy (i.e., 42.4 kJ m^{-2}), which is the highest performance reported so far. Moreover, this fabrication technique fully meets the requirements of the classical wet spinning using the non-solvent-induced phase separation, and can therefore be innovatively applied to prepare continuous eutectogel fibers for conductive sensing and engineering materials.

2. Results and Discussion

Figure 1a depicted our consecutive fabrication process of the tough PVA eutectogel with a homogeneous structure. Concretely, a perfect "polymer dissociation" was first achieved by dissolving PVA in water, since the strong hydrogen bonding between water molecules and the hydroxyl groups of PVA inhibited the expression of the initial polymer–polymer interactions (Figures S1a and S2, Supporting Information). Afterward, because of the poor interactions between PVA and DESs molecules (Figure S1b, Supporting Information), replacing water with DESs enhanced the expression of the polymer-polymer interactions and promoted the formation of small-sized, uniformly distributed crystals in the PVA network that acted as cross-linking points, thus completing the "network reconstruction". Driven by the spatiotemporal expression of polymer interactions in water and DESs, a homogeneous and robust physical cross-linking network could be established, and the obtained PVA eutectogel (DESs-PVA) exhibited outstanding deformability yet high strength (Figure 1b,c). Moreover, by adjusting the content of PVA (10, 15, and 20 wt.%), it was possible to generate a series of PVA eutectogels (DESs-PVA_x, x represents the weight fraction of PVA aqueous solution) with tunable properties. To highlight the virtue of the spatiotemporal expression of polymer interactions regulated by solvent-replacement strategy,

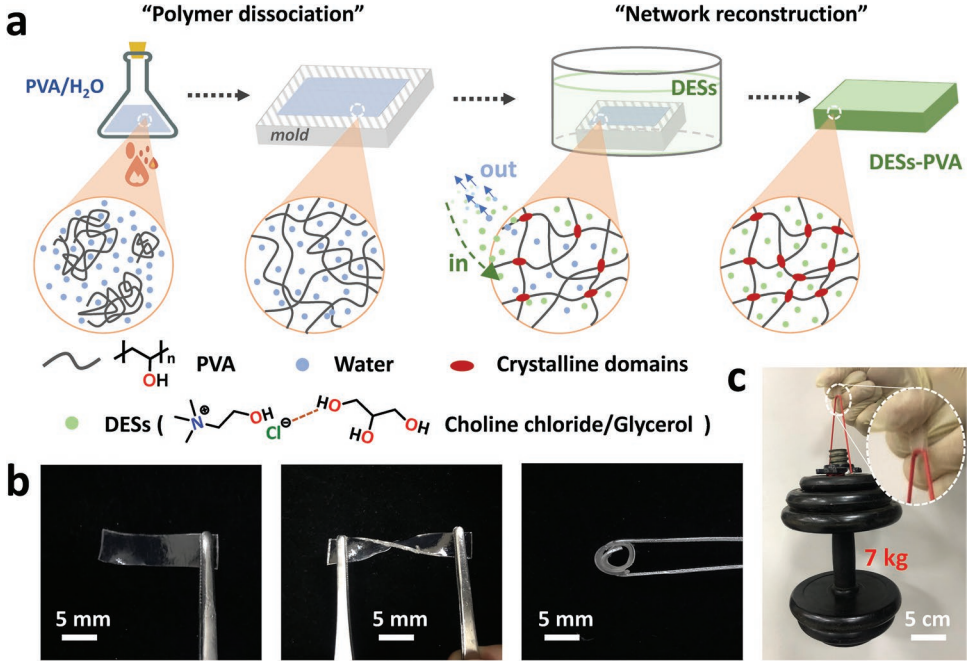

Figure 1. Fabrication and performance exhibition of DESs-PVA eutectogel. a) Schematic illustration of the consecutive preparation process of DESs-PVA eutectogel by the solvent-replacement approach. First, PVA was dissolved in water to disrupt the polymer–polymer interactions to obtain an aqueous solution with uniform polymer distribution, namely, "polymer dissociation". Afterward, the PVA aqueous solution was transferred into DESs (choline chloride/glycerol = 1/2, molar ratio) for replacing water to strengthen the interactions between PVA, facilitating the formation of a large number of crystal domains as cross-linking points in the "network reconstruction". b) Photographs of transparent DESs-PVA_{15} eutectogel that can be twisted and crimped. c) Photograph illustrated the remarkably high strength of DESs-PVA_{15} (50 mm × 5 mm × 2 mm), by withstanding a 7 kg dumbbell without any deformation.

a PVA eutectogel (HC-PVA$_{10}$) with a weight fraction of 10 wt.% was prepared as a control by the traditional heating–cooling method.[23,30,31] Because PVA was poorly soluble in DESs, it could only be fully dissolved when the temperature rose to 150 °C (Figure S3a, Supporting Information). Once this heated PVA/DESs solution was allowed to cool to room temperature, it rapidly solidified yielding solid-like opaque HC-PVA$_{10}$ (Figure S3b and Video S1, Supporting Information).

Thermogravimetric analysis (TGA) confirmed that the free water in DESs-PVA obtained by solvent-replacement was completely removed, leaving only a small amount of bound water (Figure S4, Supporting Information). Moreover, the molar ratio of glycerol to choline chloride in DESs-PVA was still 2:1, as proved by ^{1}H NMR spectrum (Figure S5, Supporting Information). Subsequently, the changes of the polymer skeleton before and after the solvent-replacement were observed by scanning electron microscopy (SEM, Figure S6, Supporting Information). After freeze-drying, the PVA solution presented a loose stacked sheet structure, which was attributed to the lack of strong cross-linking between PVA chains. In contrast, a continuous 3D network structure was established in the DESs-PVA, due to the enhanced inter-polymer interactions after solvent-replacement.[32] The attenuated total reflection Fourier transform infrared (ATR-FTIR) spectroscopy was used to investigate the hydrogen bonding between polymers within DESs-PVA and HC-PVA$_{10}$ (**Figure 2**a; Figure S7, Supporting Information). For HC-PVA$_{10}$, the broad peak at 3335 cm^{-1} was assigned to the stretching vibration of O—H (ν_{O-H}) on PVA and glycerol. On the contrary, the ν_{O-H} of DES-PVA appeared at a lower wavenumber region and further moved to 3301 from 3315 cm^{-1} as the PVA content increased from 10 to 20 wt.%. It was widely established that the intra/intermolecular hydrogen bonding between PVA can lower the force constants of chemical bonds, resulting in a red-shift in their vibrational frequencies.[33] Thus, the shift of ν_{O-H} implied that the polymer–polymer interactions has been reinforced from HC-PVA$_{10}$ to DESs-PVA$_{20}$. In other words, the solvent-replacement was crucial to boost the expression of the polymer interactions. To further confirm this

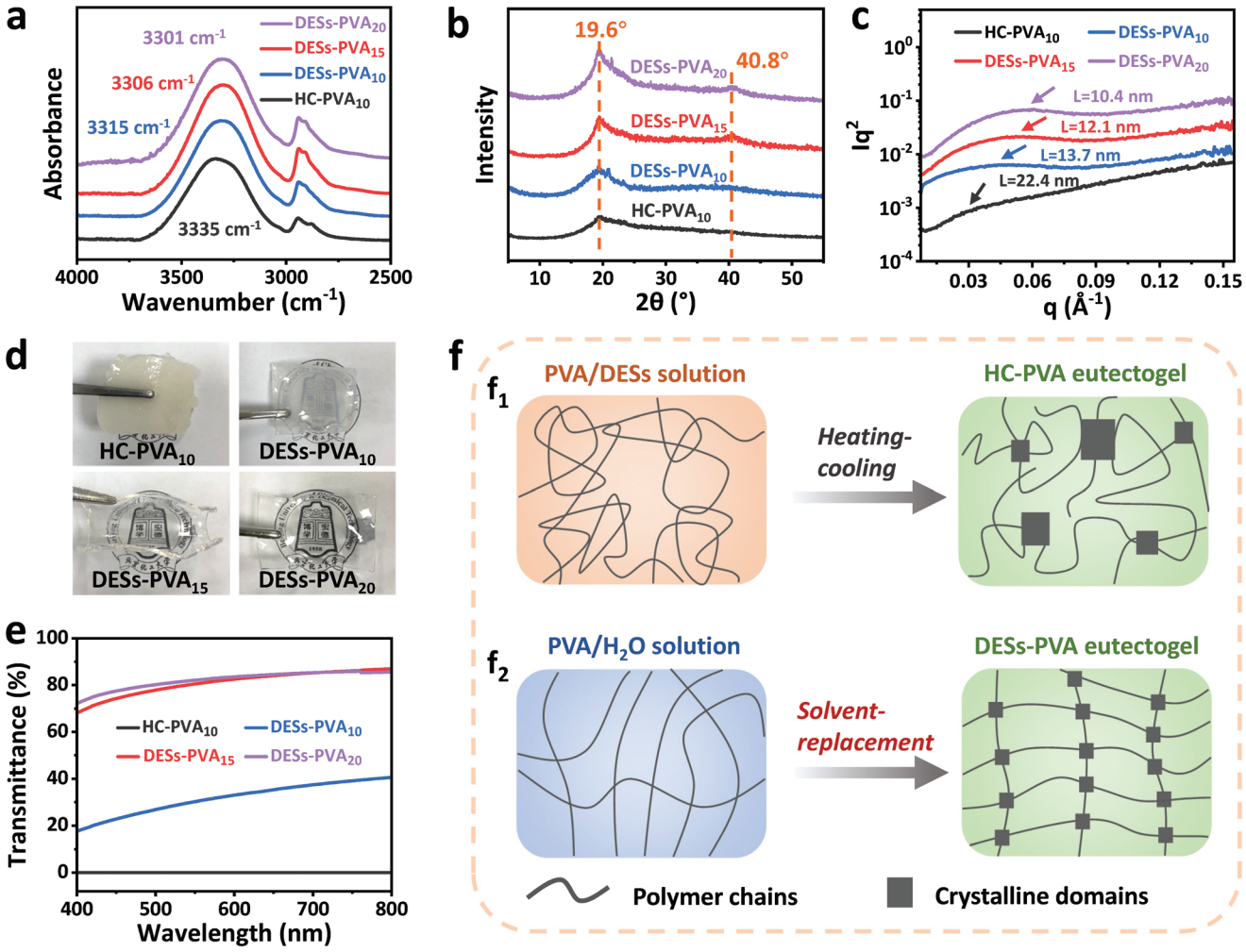

Figure 2. Mechanistic investigation for the formation of DESs-PVA eutectogel. Comparison of a) ATR-FTIR spectra, b) WAXS patterns, and c) SAXS patterns. d) Photographs of the HC-PVA$_{10}$ and DESs-PVA eutectogel. HC-PVA$_{10}$ was opaque while DESs-PVA eutectogel had a high degree of transparency that was improved with the increasing PVA content. e) Transmittance spectra of HC-PVA$_{10}$ and DESs-PVA eutectogel with different PVA contents (10, 15, 20 wt.%). f) Schematic diagrams of the network structure of HC-PVA$_{10}$ and DESs-PVA eutectogel during the evolution from sol to gel, highlighting the different cross-linking density and crystal domains.

inference, a peak fitting method was performed on the region of ν_{O-H} from 3000 to 3800 cm^{-1}, where the peak at 3210 cm^{-1} was attributed to the PVA–PVA interactions (Figure S8a–d, Supporting Information).[28] And the contribution of the hydrogen bonding between PVA was quantified by calculating the area ratio of the peak at 3210 cm^{-1} to the sum area of ν_{O-H} (Figure S8e, Supporting Information). The lowest area ratio (20.7%) of HC-PVA_{10} suggested that the hydrogen bonding between PVA was more obvious in DESs-PVA eutectogel. Furthermore, the hydrogen bonding inside the DESs-PVA eutectogel was continuously enhanced with rising PVA content from 10 to 20 wt.%.

Subsequently, the structures of HC-PVA_{10} and DESs-PVA eutectogel were determined by wide-angle X-ray scattering (WAXS) and small-angle X-ray scattering (SAXS) to evaluate the effect of "network reconstruction". As shown in Figure 2b, the WAXS signals of HC-PVA_{10} merely exhibited a single blunt peak at 19.6°, which corresponded to the average lateral distance of 0.45 nm between molecules without special organization. However, the signals of DESs-PVA_x ($x = 10$, 15, 20) became sharper with increasing value of x, indicating a rise in crystallinity. Among DESs-PVA_{20}, eutectogel presented two obvious diffraction peaks at $2\theta = 19.6°$ and 40.8°, corresponding to the (101) and (102) planes of PVA crystallites.[34,35] This difference in crystallinity could also be observed intuitively by polarizing optical microscopy, with significant birefringence in the high crystalline DESs-PVA, but not in the HC-PVA_{10} (Figure S9, Supporting Information). According to the SAXS profile (Figure 2c), the distance (L) between the adjacent crystallites was calculated to be 22.4, 13.7, 12.1, and 10.4 nm for HC-PVA_{10}, DESs-PVA_{10}, DESs-PVA_{15}, and DESs-PVA_{20}, respectively. Their average crystallite size (R_g) was analyzed by applying the Guinier equation,[36] where the crystallite in HC-PVA_{10} was ≈4.06 nm, larger than that of DESs-PVA_{10} (3.86 nm), DESs-PVA_{15} (3.53 nm), and DESs-PVA_{20} (2.95 nm) (Figure S10, Supporting Information). That is to say, PVA tended to crystallize and formed small-scale crystal structures following the solvent-replacement process, and the crystal size reduced further as PVA contents increased. Therefore, it was reasonable to conclude that the polymer cross-linking network within DESs-PVA was denser and the distance between adjacent cross-linking sites (crystallites) was shorter compared to that of HC-PVA_{10}.

It is worth noting that the prepared HC-PVA_{10} eutectogel was opaque, while the DESs-PVA eutectogel exhibited high transparency (Figure 2d), which can be tuned by varying PVA concentration, with an abrupt transition of transmission at 550 nm from nearly 25% for DESs-PVA_{10} to Σ85% for DESs-PVA_{20} (Figure 2e). It is generally accepted that the uniform distribution of crystals with regular structure and tiny size provides PVA gel with excellent transmittance, owing to the fact that they can reduce the occurrence of light scattering and improve the optical transmittance of the gel by enhancing light refraction.[37,38] We believed that the improved transmittance in DESs-PVA was attributed to the formation of a more uniform internal polymer network with smaller crystal structures as illustrated in Figure 2b,c and Figure S10 (Supporting Information). In the case of HC-PVA_{10} eutectogel, due to the poor compatibility between PVA and DESs, severe phase separation may occur in the heating–cooling process with a generation of faulty large-size crystal, causing intense light scattering in opaque HC-PVA_{10}. According to the foregoing results, while heating in DESs could disrupt the polymer interactions and achieve the "polymer dissociation" of PVA, the subsequent cooling process did fail to restore the broken internetwork connections, that is, the required "network reconstruction" would not happen in the HC-PVA_{10} (Figure 2f_1). Nevertheless, adopting the solvent-replacement technique could easily and efficiently modulate the spatiotemporal expression of polymer interactions, allowing PVA to be "dissociated" in water by weakening polymer interactions according to the mind, and could also enhance polymer interactions in time to induce the formation of uniformly distributed, small-sized PVA crystals, thereby reconstructing a homogeneous, robust polymer network (Figure 2f_2).

The macroscopic mechanical behaviors of the as-prepared eutectogels were comparatively investigated using an electronic tensile machine with a 500-N load cell at a stretching rate of 100 mm min^{-1}. Due to the shortage of a robust polymer network for energy dissipation, the HC-PVA_{10} showed particularly weak tensile performance. As shown in **Figure 3**a, DESs-PVA_{10} had a stress of 6.6 MPa and a strain of 550%, which was a great deal better than those of HC-PVA_{10} (0.3 MPa and 150% for HC-PVA_{10}). With the content of PVA increased to 15 and 20 wt.%, the ultimate stress remarkably raised and attained 12.2 MPa for DESs-PVA_{15}, as well as 20.2 MPa for DESs-PVA_{20}. It could also be seen from the stress–strain curve that the DESs-PVA eutectogel has undergone two different strain regions. Below 50% strain, the DESs-PVA was in the elastic region, and its deformation mainly came from the movement of small-scale units such as bond length or bond angle in the polymer chains. When the strain was higher than 50%, the DESs-PVA was in the strain-hardening region, and the polymer chains began to move and orientate under external forces, leading to a rapid increase in strain and stress. Moreover, Young's modulus and toughness also increased monotonically with increasing PVA content, reaching 16.1 MPa and 62.7 MJ m^{-3} in DESs-PVA_{20}, which were 100 and 570 times higher than those of HC-PVA_{10} (0.16 MPa and 0.11 MJ m^{-3}, Figure 3b). In terms of mechanical characteristics, DESs-PVA eutectogel was so brilliant that they could even be cut into an auxetic material with special topology by laser, affording a negative Poisson's ratio in tensile mode (Figure S11 and Video S2, Supporting Information). Figure 3c demonstrates the comparison plot of the maximum stress and the toughness with typical eutectogels and ionogels. Obviously, the DESs-PVA eutectogel outperformed existing synthetic eutectogels and ionogels, including PVA/poly(acrylic acid) (PAA) eutectogel,[23] poly(N-hydroxyethylacrylamide) (PHEAA)/bisgluconamide bolaamphiphilic (BGA) eutectogel,[39] gelatin eutectogel,[40] PAA/cellulose nanocrystals (CNC) eutectogel,[41] PAA/poly(acrylamide) (PAAm) ionogel,[42] poly(N,N-dimethylacrylamide) (PDMAA)/poly(1-acrylamido-2-methylpropane sulfonic acid) (PAMPS) ionogel,[43] poly(ethylene glycol methyl ether acrylate) (PMEA)/poly(isobornyl acrylate) (PIBA) ionogel,[44] block polymer ionogel,[45] and poly(2,2,2-trifluoroethyl acrylate-co-acrylamide) [poly(TFEA-co-AAm)] ionogel.[46] Noteworthy, to the best of our knowledge, the ultimate stress (20.2 MPa) and the toughness (62.7 MJ m^{-3}) of the DESs-PVA_{20} eutectogel are the highest values among the reported physical eutectogels and hold potentials to be further promoted. This is due to the

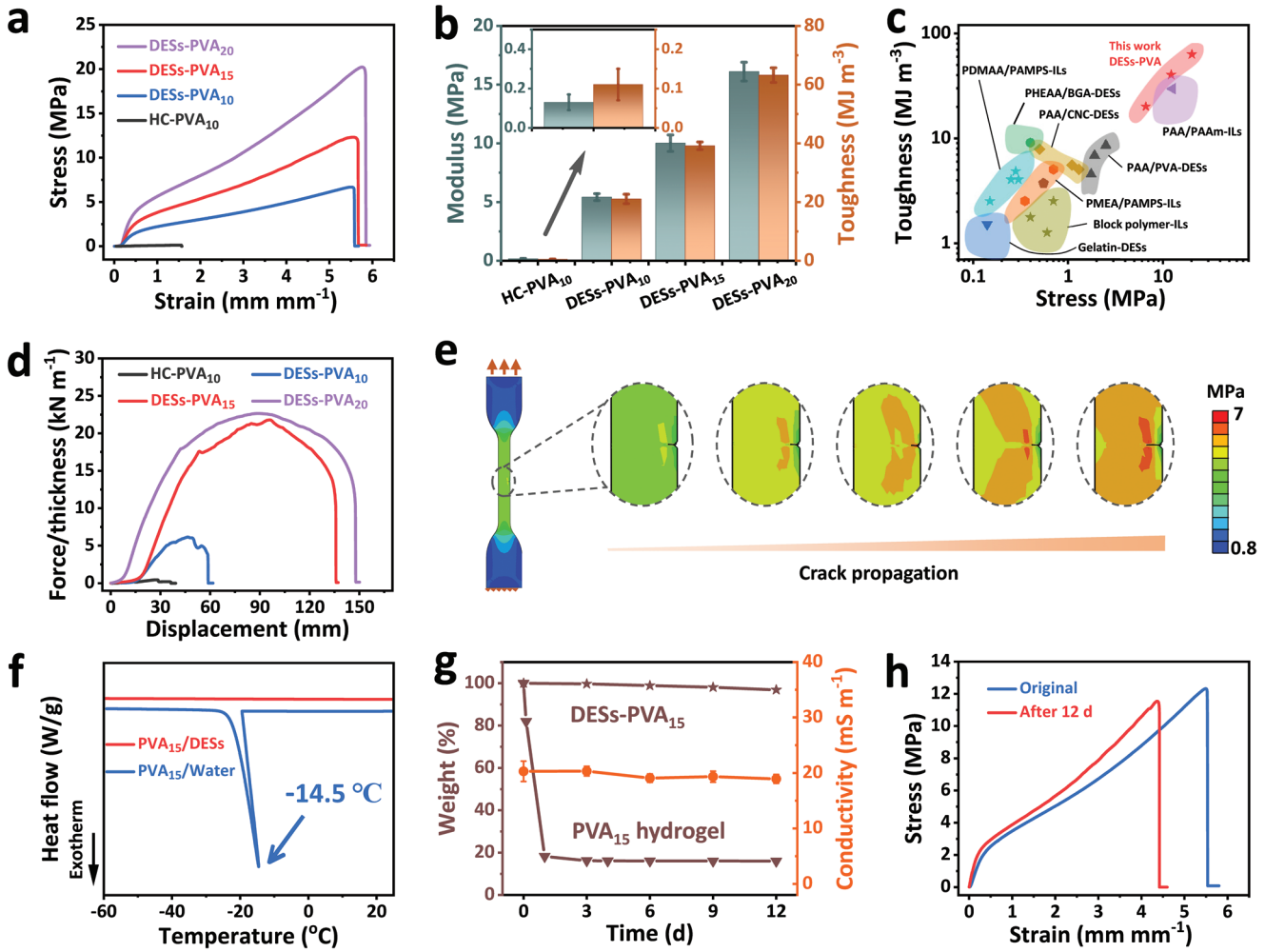

Figure 3. Mechanical and temperature-resistant properties of the DESs-PVA eutectogel. a) Tensile stress–strain curves and b) the corresponding modulus and toughness of the DESs-PVA and HC-PVA_{10} eutectogel. c) Comparison of the stress and toughness of DESs-PVA with other reported eutectogels and ionogels. d) Tearing curves of the HC-PVA_{10} and DESs-PVA eutectogel. e) Finite element simulation of the stress distribution inside the DESs-PVA_{15} eutectogel during crack propagation. The scale bar from red to blue indicated that the stress concentration was from high to low. f) DSC curves of DESs-PVA_{15} eutectogel versus PVA_{15} hydrogel using pure water as solvent during the cooling process from 25 to –60 °C. g) Weight and conductivity change plots of the DESs-PVA_{15} eutectogel and PVA_{15} hydrogel stored at 20–25 °C and 30–40% humidity. h) Tensile stress–strain curves of the DESs-PVA_{15} before and after exposure to the environment (20–25 °C and 30–40% humidity) for 12 days. The error bars represent standard deviation; sample size $n = 3$.

fact that the DESs content in DESs-PVA_{20} could reach 56.2% (Figure S12, Supporting Information), implying its stress could be further theoretically enhanced as long as the concentration of PVA in water can be enriched. Without a doubt, since the lower content of DESs also caused a reduction in ionic conductivity of eutectogel (Figure S13, Supporting Information), a suitable composition must be determined ahead of time.

Additionally, we evaluated the tearing properties of eutectogels by trouser tearing tests (Figure S14, Supporting Information),[47,48] where a similar trend was observed for tearing strength (Figure 3d). After calculation, tearing the DESs-PVA eutectogel needed a substantial amount of energy, with 10.9 ± 0.6 kJ m^{-2} for DESs-PVA_{10}, 38 ± 2.3 kJ m^{-2} for DESs-PVA_{15}, and 42.4 ± 4.0 kJ m^{-2} for DESs-PVA_{20} (Figure S15, Supporting Information), which was roughly 11, 28, and 43 times that of the HC-PVA_{10}, respectively. The tearing energy of DESs-PVA_{20} set another record compared with existing eutectogels and ionogels (the maximum values of eutectogels and ionogels in previous reports[39,49] were Σ1.4 and Σ24 kJ m^{-2}, respectively). This high tearing energy consumption indicated that the DESs-PVA eutectogel continued to function well in resisting crack propagation. In addition to the presence of strong polymer networks, the crystalline domains delayed the fracture of individual polymer chains by crack pinning, which was another reason for the tear-resistance enhancement (Figure S16, Supporting Information).[25,50] Then, we verified the presumption by finite element analysis (FEA). As shown in FEA diagrams (Figure 3e; Figure S17, Supporting Information), the tip stress raised with increasing crystallinity inside the eutectogels, effectively illustrating the role of the crystal zone in dissipating fracture energy.[26]

Taken in sum, modulating the spatiotemporal expression of non-covalent interactions between polymers by the simple and

efficient solvent-replacement approach was helpful for overcoming the contradictions of polymer interactions in polymer solvation and cross-linking processes, which resulted in satisfactory "dissociation" and "reconstruction" of polymer networks to gain highly strong and tough DESs-PVA eutectogel with excellent tear resistance.

Benefiting from the inherent low freezing point and nonvolatile features of DESs, the DESs-PVA eutectogel also exhibited good anti-freezing and anti-drying performances. The freezing temperature was measured by differential scanning calorimetry (DSC) to highlight the anti-freezing ability. As shown in Figure 3f, a sharp peak located at −14.5 °C as the freezing point of free water was observed for PVA hydrogel with pure water as the solvent, while no exothermic peak appeared even at −60 °C for DESs-PVA_{15} eutectogel, which still maintained flexibility and could be twisted easily after storing at −18 °C for 7 days (Figure S18, Supporting Information). Moreover, the DESs-PVA eutectogel demonstrated much better solvent retention properties than the PVA hydrogel. After 12 days of storage at room temperature, the DESs-PVA_{15} underwent a slight mass loss (Σ3.1%) and its conductivity remained stable, while the PVA_{15} hydrogel has already lost the majority of water within 24 h due to the evaporation (Figure 3g). According to the stress–strain curves in Figure 3h, there was no substantial change in stress for DESs-PVA_{15} after 12 days, albeit a little fall in strain from 550% to 450%. This was primarily due to the high stability of both the internal crystal structure and DESs over time (Figures S19 and S20, Supporting Information). All these results confirmed the temperature-resistant properties of the DESs-PVA eutectogel, which was conductive to avoid degradation of their performance under extreme environments.

The repairability experiment showed that DESs-PVA eutectogel could be repaired after applying PVA aqueous solution to the damaged area and gelling it with fresh DESs. As demonstrated in **Figure 4**a as well as Figures S21a and S22a (Supporting Information), the physical hole in the DESs-PVA was fully filled and the eutectogel basically returned to its original shape. The repair efficiency was defined as the ratio of the strength of the repaired sample over the initial strength of the original sample. After repair, the fracture strength of DESs-PVA_{10}, DESs-PVA_{15}, and DESs-PVA_{20} was 5.1, 8.7, and 12.2 MPa, respectively, with the repair efficiency exceeding 60% (Figure 4b; Figures S21b and S22b, Supporting Information). Figure 4c illustrates the entire repair process. When the PVA aqueous solution contacted the fracture surface of the DESs-PVA eutectogel, the water and DESs would interpenetrate to form a transition zone in which the original polymer interactions were weakened and the PVA in water gradually migrated into the zone, resulting in a gradual enrichment of the PVA content. Following that, the full replacement of water in the transition zone by DESs was able to restore the weakened polymer interactions, forming new bonding interactions and completing the network repair. Such repairability would greatly extend the cycle-life and durability of the DESs-PVA eutectogel used as engineering and functional materials.

Along with the robust mechanical, temperature-tolerance, and repairable properties, the DESs-PVA eutectogel exhibited extraordinary adhesion to a variety of substrates, including wood, glass, poly(methyl methacrylate) (PMMA), polystyrene (PS), polytetrafluoroethylene (PTFE), and metal plates (aluminum and copper). As illustrated in **Figure 5**a, the PVA aqueous solution was first applied dropwise to the surface of

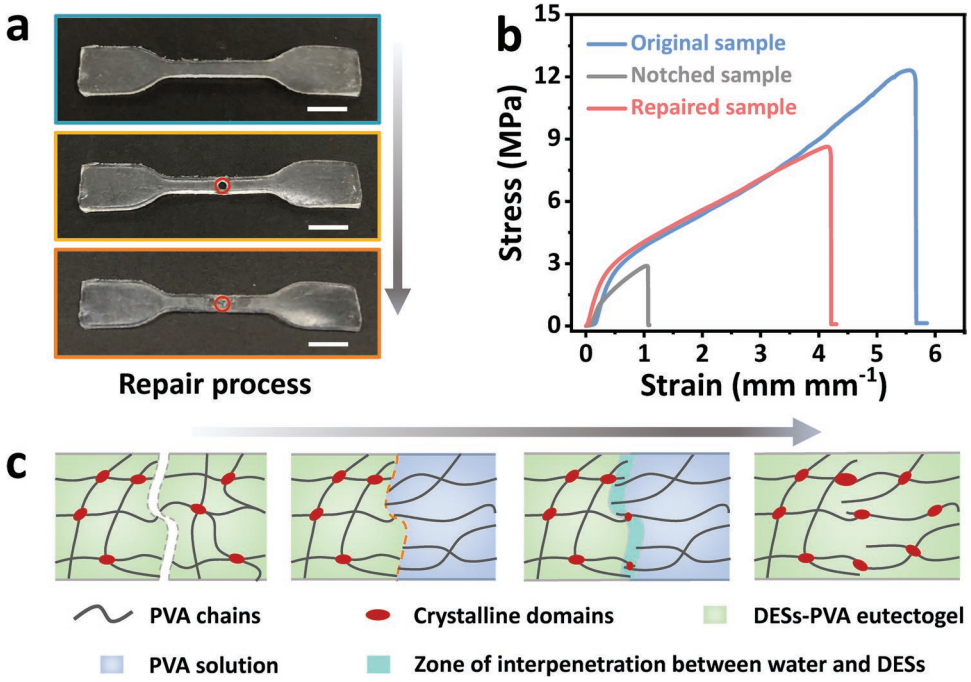

Figure 4. Repairability of DESs-PVA eutectogel. a) Photographs demonstrating the facile repairability of DESs-PVA_{15}. From top to bottom were photographs of the intact DESs-PVA_{15} and its disrupted and repaired form. Scale bar was 5 mm. b) Tensile curves of the original, notched, and repaired DESs-PVA_{15}. c) Schematic representation of the repairable process of DESs-PVA eutectogel.

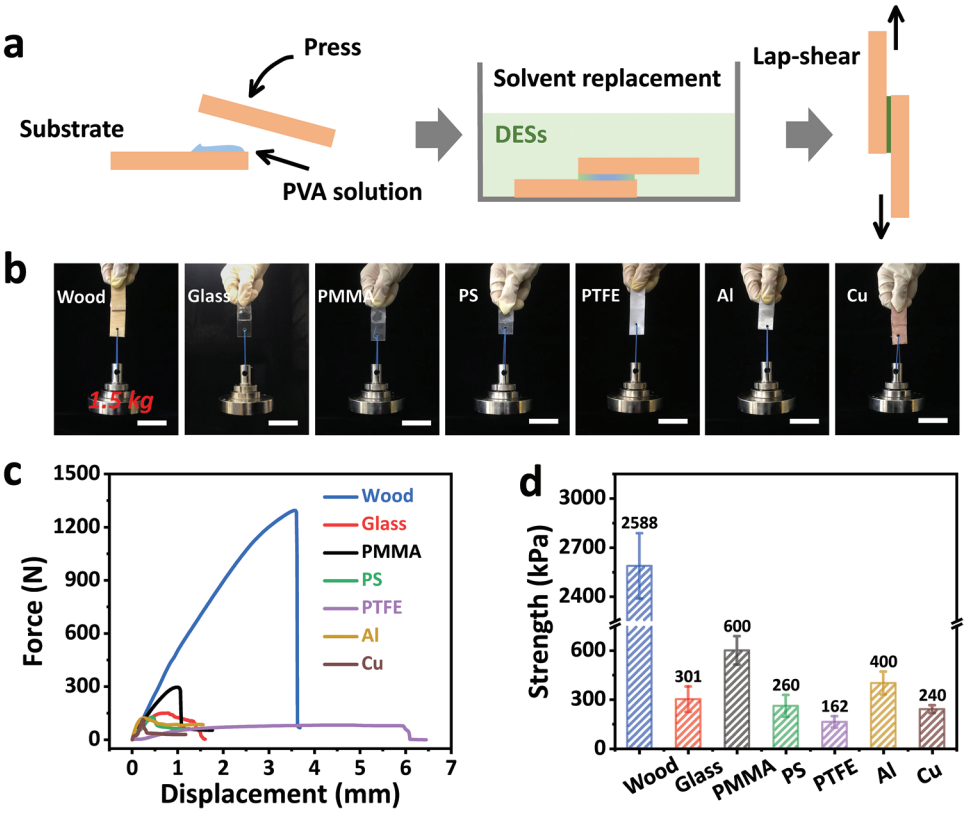

Figure 5. Adhesion characterizations of the DESs-PVA eutectogel. a) Schematic illustration of the adhesion test for DESs-PVA eutectogel. b) Photographs of the DESs-PVA_{15} eutectogel adhering to diverse substrates, which can easily withstand a weight of 1.5 kg hanging on both hydrophilic and hydrophobic surfaces. Scale bar was 5 cm. c) Lap-shear curves and d) the corresponding adhesion strength of different substrates adhered by DESs-PVA_{15} eutectogel. The error bars represent standard deviation; sample size $n = 3$.

one substrate and then covered with the other substrate after complete spreading. Upon the solvent-displacement treatment, a strong eutectogel bonding layer formed between two substrates. Figure 5b showed that a weight up to 1.5 kg was attached to one of the two plates glued together on a 5 cm^2 area by DESs-PVA_{15} eutectogel, and no observable sliding between these two plates by shear forces was detected. Lap-shear tests revealed that the DESs-PVA_{15} eutectogel adhered best to the wood surface compared to the other tested surfaces (Figure 5c; Figure S23, Supporting Information), which could even bear an adult (Σ65 kg) without detaching (Video S3, Supporting Information). The adhesion strength of DESs-PVA_{15} eutectogel to different substrates is measured and displayed in Figure 5d, with 2588 kPa for wood, 301 kPa for glass, 400 kPa for aluminum, and 240 kPa for copper. Moreover, good adhesion was also found on hydrophobic surfaces, for example, 600 kPa at PMMA, 260 kPa at PS, and 162 kPa at PTFE. By virtue of the inherent temperature-resistance of the eutectogel, its adhesion was well maintained over a wide temperature range from −18 to 60 °C (Figure S24, Supporting Information). Adhesive experiments conducted over a period of 12 days also indicated that the adhesion strength of the DESs-PVA_{15} eutectogel did not diminish, highlighting its long-term adhesion stability (Figure S25, Supporting Information).

The extraordinary adhesive properties of the DESs-PVA eutectogel were most likely caused by two factors (Figure S26, Supporting Information). Before the solvent displacement, PVA chains were distributed as free chains in water, so they were able to deform or migrate to make full contact with the substrate surface and form strong interfacial interactions through multiple hydrogen bonding and omnipresent van der Waals interactions. After the solvent displacement, the charged choline chloride/glycerol molecules were introduced to the bonding layer to enhance interfacial interactions through electrostatic, ion–dipole interactions, and metal complexation. Moreover, the robust polymer networks were formed to provide strong cohesion. The synergistic contribution of multiple inherent interfacial interactions and strong cohesion of the DESs-PVA_{15} eutectogel led to the outstanding adhesion.[39] Certainly, the adhesive strength can also be artificially regulated by appropriately adjusting the contents of PVA (Figure S27, Supporting Information).

Due to the enhanced hydrogen bonding between polymers induced the phase separation, this solvent-displacement strategy offered a suitable window for the continuous production of eutectogel fibers, which had the similar process requirements for conventional wet spinning.[51] **Figure 6**a illustrated the wet-spinning process of eutectogel fibers. The PVA aqueous solution was simply injected into a DESs solution by a syringe, where it quickly solidified to eutectogel fibers as the water diffused out (Video S4, Supporting Information). With a fast extrusion process and moderate draft ability, it was not a challenge

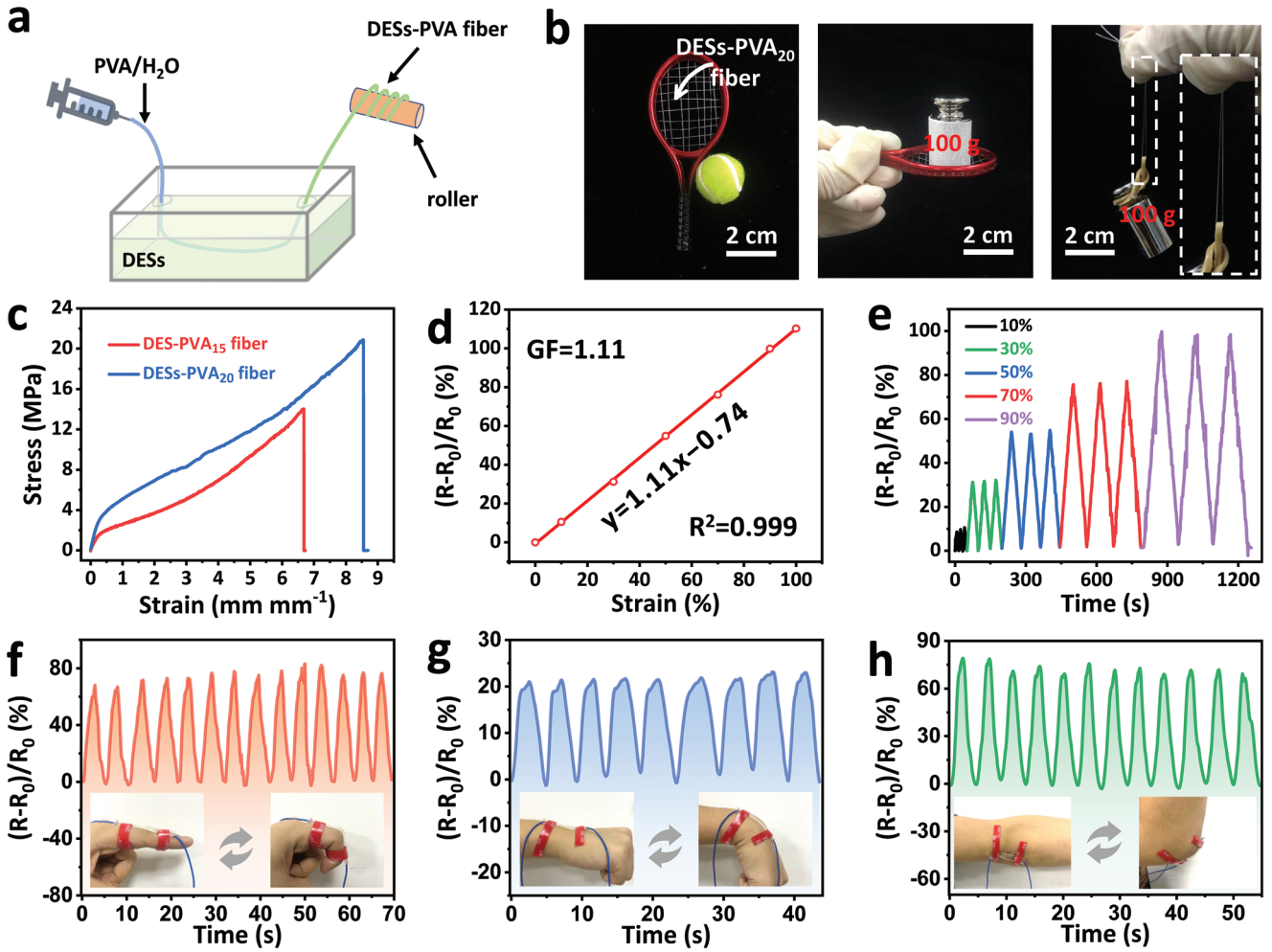

Figure 6. Fabrication of DESs-PVA eutectogel fiber. a) Schematic illustration of the preparation of DESs-PVA eutectogel fiber by the solvent-replacement strategy. b) Photographs of DESs-PVA_{20} fiber woven on a model of tennis racket and its load-bearing capacity. Both the compiled mesh and the single fiber can withstand a weight of 100 g. c) Tensile strain–stress curves for the DESs-PVA_{15} fiber and DESs-PVA_{20} fiber. d) Resistance-strain curve of the DESs-PVA_{15} fiber sensor within 100% strain and the corresponding GF value ($R^2 = 0.999$). e) Relative resistance changes under cyclic strains from 10% to 90% as the stretching rate of 20 mm min^{-1}. Monitoring three continuously moving joints: f) finger, g) wrist, and h) elbow. The insets show the fiber sensor adhered onto the corresponding joint sites.

to manufacture continuous eutectogel fibers in large scale (Figure S28, Supporting Information). The obtained eutectogel fibers were readily woven into textiles and provided an excellent load-bearing function (Figure 6b), showing potentials to be integrated with conventional fabrics as engineering materials. Under the same extrusion rate, the diameter of eutectogel fiber was mostly determined by the PVA concentration, i.e., 187 ± 7 µm for DESs-PVA_{15} fiber, while 382 ± 10 µm for DESs-PVA_{20} fiber (Figure S29, Supporting Information). As the extrusion force promoted the orientation of PVA chains, eutectogel fiber outperformed the bulk material in mechanical performance. The maximum strain of DESs-PVA_{20} fiber even reached 850% (Figure 6c; Figure S30, Supporting Information).

These stretchable conductive eutectogel fibers with dynamic mechanical properties were good candidates for strain sensors (Figure S31, Supporting Information). In general, sensitivity and stability were important for strain sensors. The gauge factor (GF), defined as the change in relative resistance with applied strain, was used to represent the sensitivity of sensors.[52,53] Figure 6d shows the resistance change versus the increasing of strain (0–100%), revealing an excellent linear relationship ($R^2 = 0.999$) and a high gauge factor of 1.11. The cyclic stretching and releasing tests under 10–90% strain demonstrated an increased resistance change proportional to the tensile strain (Figure 6e), confirming that the sensor could output reliable resistance signals and systematically detect physical deformation. In addition, the fiber sensor exhibited good operational stability as the electrical signal was stable enough upon repetitive cycles at 40% strain for 2000 s (Figure S32, Supporting Information).

Since the fiber sensor displayed good sensing sensitivity and signal repeatability for various deformations, it was suitable for the direct detection of complex human motions in real time. The eutectogel fiber sensor was attached to the outer skin of different joints on the body with 3 M VHB tape. With the bending movement of the joint, the sensor was stretched and

the ion migration path was prolonged (Figure S33, Supporting Information). As a result, the sensor generated a corresponding resistance signal change for the joint movement. As shown in Figure 6f–h, the repetitive bending deformation of forefinger, wrist, and elbow, all could be tracked by eutectogel fiber sensor, with showing diverse signals of relative resistance. These signal curves hold reliable repeatability and recognition characteristics, which would satisfy the demand in the preparation of motion monitoring devices for human daily exercise and make a good application prospect in the field of postural correction and joint diagnosis.

Given the benefits of the solvent-regulated spatiotemporal expression of polymer–polymer interactions in the preparation of high strength and tough eutectogels, we envisioned using other water-soluble polymers as backbones to create eutectogels for evaluating the universality of this approach. Physical eutectogels from gelatin (10 wt.%), carboxymethyl chitosan (CMCS, 10 wt.%), sodium carboxymethyl cellulose (CMC-Na, 10 wt.%), and sodium alginate (SA, 5 wt.%) were prepared through the solvent-replacement (named DESs-polymer$_x$, x represents the weight fraction of polymer aqueous solution) and the heating–cooling method (named HC-polymer$_x$, x represents the weight fraction of the polymer), respectively. As shown in Figure S34 (Supporting Information), the DESs-Gelatin$_{10}$ gave a fracture strength as high as Σ4 MPa, which was substantially higher than that of HC-Gelatin$_{10}$. Likewise, DESs-CMCS$_{10}$, DESs-CMC-Na$_{10}$, and DESs-SA$_5$ overwhelmingly exceeded the corresponding HC-CMCS$_{10}$, HC-CMC-Na$_{10}$, and HC-SA$_5$ in terms of mechanical properties. In addition, these four eutectogels also maintained good electrical conductivity and high solvent content (Figure S35, Supporting Information). These results implied that the solvent-replacement principle can be applied to other polymers and DESs, and would greatly promote the development of physical eutectogels.

3. Conclusion

We devised a simple and universal solvent-replacement method for regulating the spatiotemporal expression of non-covalent interactions between polymers, thus manufacturing strong and tough PVA eutectogel (DESs-PVA) with homogenous and robust networks. The obtained DESs-PVA eutectogel exhibited superb mechanical strength (20.2 MPa), toughness (62.7 MJ m^{-3}), and tearing energy (42.4 kJ m^{-2}), surpassing all currently reported physical polymer eutectogels. Benefiting from the inherent advantages of DESs, the eutectogels demonstrated wide temperature-tolerance and good conductivity, which can replace temperature-resistant hydrogels and expensive ionogels as alternative flexible ionic conductors. The DESs-PVA eutectogel was also repairable, significantly extending its cycle-life and durability used as engineering and functional materials. In addition, the in situ gelation induced by the solvent-displacement method made the eutectogel suitable for the fabrication of high-strength adhesives and continuous conductive fibers. The present work provides a promising strategy to manufacture mechanically robust and functionally integrated smart materials for the next-generation of soft electronic devices and engineering applications with high environmental adaptability.

4. Experimental Section

Preparation of Deep Eutectic Solvents (DESs): Under a temperature condition (90 °C), DESs were made by mixing choline chloride (ChCl) and glycerol (Gly) in a molar ratio of 1:2 until a homogenous and transparent solution was obtained.

Preparation of DESs-PVA Eutectogel: To make DESs-PVA eutectogel, the solvent-displacement approach was used. PVA powders (3, 4.5, and 6 g) were initially dissolved in pure water (27, 25.5, and 24 g) at 95 °C with stirring for 3 h until the clear PVA aqueous solutions formed with mass fraction of 10, 15, and 20 wt.%. After defoaming, the transparent solutions (10 mL) were poured into glass molds (thickness is 2 mm) and submerged in 500 mL of DESs for 18 h to create the DESs-PVA$_x$ eutectogel (*x* refers to the mass fraction of PVA, 10, 15, and 20 wt.%). Every 6 h, the DESs was changed with new DESs to ensure that the water was completely replaced.

Preparation of HC-PVA Eutectogel: HC-PVA eutectogel was prepared through the traditional heating–cooling method. Briefly, 3 g of PVA powder was dissolved into 27 g of DESs (ChCl/Gly) at 150 °C under stirring until being completely dissolved. After that, the solution was transferred into glass molds (thickness is 2 mm) to solidify at room temperature.

Fabrication of DESs-PVA Eutectogel Fiber: The PVA aqueous solution (15 and 20 wt.%) was loaded in a 10 mL syringe and spun into the coagulation bath (305 × 70 × 75 mm^3) containing 500 mL of DESs through a steel needle (18 G). The flow rate of the PVA solution was maintained at 0.3–0.4 mL min^{-1} using a microinjection pump (LSP04-1A, Longer Precision Pump Co., Ltd.). The prepared eutectogel fibers were collected manually by plastic drum, and no drafting was produced during collection. Since the viscosity of the PVA solution with a mass fraction of 10% was too low to form a continuous liquid flow in the DESs coagulation bath, the corresponding eutectogel fibers were not obtained.

Design and Characterization of Eutectogel Fiber Sensor: DESs-PVA$_{15}$ eutectogel fiber with a length of 5 cm were sandwiched between two 3 M VHB adhesive tapes for the assembly of fiber sensor. The copper tape at both ends of the fibers was used to connect the fibers sensor with output metallic wires. A digital source meter (B35T+, OWON) was used to measure the real-time resistance of the fiber sensor under different strains. The relative resistance change was determined from $(R–R_0)/R_0 \times 100\%$, where R refers to the dynamic resistance under different strains and R_0 denotes the initial resistance. The strain sensitivity of fiber sensor was calculated by gauge factor (GF), as defined by the ratio of the relative resistance change rate to the applied strain (ε), i.e., $GF = (\Delta R/R_0)/\varepsilon$. The fiber sensor was attached to various joints of human body by 3 M VHB tape to complete the human motions monitoring experiments. The real-time resistance change was monitored on an electrochemical workstation (CHI760E, CH Instruments) at 0.4 V voltage. All human sensing demonstrations were performed in Beijing University of Chemical Technology (China), where the project was fully assessed and approved by the university ethic committee with the consent issued from the participant.

Supporting Information

Supporting Information is available from the Wiley Online Library or from the author.

Acknowledgements

This work was supported by the Open Fund of National Key Laboratory of Science and Technology on Advanced Composite (KZ42191814).

Conflict of Interest

The authors declare no conflict of interest.

Data Availability Statement

The data that support the findings of this study are available in the supplementary material of this article.

Keywords

eutectogels, high-performance, multifunction, solvent-replacement, spatiotemporal expressions

Received: June 2, 2022
Revised: July 2, 2022
Published online:

[1] C. Yang, Z. Suo, *Nat. Rev. Mater.* **2018**, *3*, 125.
[2] J.-Y. Sun, C. Keplinger, G. M. Whitesides, Z. Suo, *Adv. Mater.* **2014**, *26*, 7608.
[3] Z. Lei, Q. Wang, S. Sun, W. Zhu, P. Wu, *Adv. Mater.* **2017**, *29*, 1700321.
[4] S. Z. Yu, A. Khademhosseini, *Science* **2017**, *356*, eaaf3627.
[5] V. R. Feig, H. Tran, M. Lee, Z. Bao, *Nat. Commun.* **2018**, *9*, 2740.
[6] C. Zhang, B. Wu, Y. Zhou, F. Zhou, W. Liu, Z. Wang, *Chem. Soc. Rev.* **2020**, *49*, 3605.
[7] J. Visser, F. P. W. Melchels, J. E. Jeon, E. M. van Bussel, L. S. Kimpton, H. M. Byrne, W. J. A. Dhert, P. D. Dalton, D. W. Hutmacher, J. Malda, *Nat. Commun.* **2015**, *6*, 6933.
[8] Y. H. Ye, Y. F. Zhang, Y. Chen, X. S. Han, F. Jiang, *Adv. Funct. Mater.* **2020**, *30*, 2003430.
[9] B. Li, J. Liu, F. Lyu, Z. Deng, B. Yi, P. Du, X. Yao, G. Zhu, Z. Xu, J. Lu, Y. Y. Li, *Adv. Funct. Mater.* **2022**, *32*, 2109302.
[10] B. Joos, J. Volders, R. R. da Cruz, E. Baeten, M. Safari, M. K. Van Bael, A. T. Hardy, *Chem. Mater.* **2020**, *32*, 3783.
[11] T. Li, Y. Wang, S. Li, X. Liu, J. Sun, *Adv. Mater.* **2020**, *32*, 2002706.
[12] B. B. Hansen, S. Spittle, B. Chen, D. Poe, Y. Zhang, J. M. Klein, A. Horton, L. Adhikari, T. Zelovich, B. W. Doherty, B. Gurkan, E. J. Maginn, A. Ragauskas, M. Dadmun, T. A. Zawodzinski, G. A. Baker, M. E. Tuckerman, R. F. Savinell, J. R. Sangoro, *Chem. Rev.* **2021**, *121*, 1232.
[13] S. E. Hooshmand, R. Afshari, D. J. Ramón, R. S. Varma, *Green Chem.* **2020**, *22*, 3668.
[14] E. L. Smith, A. P. Abbott, K. S. Ryder, *Chem. Rev.* **2014**, *114*, 11060.
[15] S. Wang, H. Cheng, B. Yao, H. He, L. Zhang, S. Yue, Z. Wang, J. Ouyang, *ACS Appl. Mater. Interfaces* **2021**, *13*, 20735.
[16] Z. Ma, J. Wang, Y. Deng, Y. Wang, L. Yan, *Biomacromolecules* **2021**, *22*, 4181.
[17] C. Gu, Y. Peng, J. Li, H. Wang, X.-Q. Xie, X. Cao, C.-S. Liu, *Angew. Chem., Int. Ed.* **2020**, *59*, 18768.
[18] J. Wu, Q. Liang, X. Yu, Q.-F. Lü, L. Ma, X. Qin, G. Chen, B. Li, *Adv. Funct. Mater.* **2021**, *31*, 2011102.
[19] J. Wang, Y. Deng, Z. Ma, Y. Wang, S. Zhang, L. Yan, *Green Chem.* **2021**, *23*, 5120.
[20] J. Ruiz-Olles, P. Slavik, N. K. Whitelaw, D. K. Smith, *Angew. Chem., Int. Ed.* **2019**, *58*, 4173.
[21] Y. Wang, Y. Liu, R. Plamthottam, M. Tebyetekerwa, J. Xu, J. Zhu, C. Zhang, T. Liu, *Macromolecules* **2021**, *54*, 3832.
[22] J. D. Mota-Morales, E. Morales-Narváez, *Matter* **2021**, *4*, 2141.
[23] Y. Wang, J. Wang, Z. Ma, L. Yan, *ACS Appl. Mater. Interfaces* **2021**, *13*, 54409.
[24] S. Jiang, L. Shang, H. Liang, B. Li, J. Li, *Food Hydrocolloids* **2022**, *127*, 107499.
[25] M. Hua, S. Wu, Y. Ma, Y. Zhao, Z. Chen, I. Frenkel, J. Strzalka, H. Zhou, X. Zhu, X. He, *Nature* **2021**, *590*, 594.
[26] X. Liang, G. Chen, S. Lin, J. Zhang, L. Wang, P. Zhang, Z. Wang, Z. Wang, Y. Lan, Q. Ge, J. Liu, *Adv. Mater.* **2021**, *33*, 2102011.
[27] S. Lin, X. Liu, J. Liu, H. Yuk, H.-C. Loh, G. A. Parada, C. Settens, J. Song, A. Masic, G. H. McKinley, X. Zhao, *Sci. Adv.* **2019**, *5*, eaau8528.
[28] L. Xu, S. Gao, Q. Guo, C. Wang, Y. Qiao, D. Qiu, *Adv. Mater.* **2020**, *32*, 2004579.
[29] L. Xu, C. Wang, Y. Cui, A. Li, Y. Qiao, D. Qiu, *Sci. Adv.* **2019**, *5*, eaau3442.
[30] Y. F. Wang, Y. Liu, R. Plamthottam, M. Tebyetekerwa, J. S. Xu, J. X. Zhu, C. Zhang, T. X. Liu, *Macromolecules* **2021**, *54*, 3832.
[31] J. Wang, B. Zhan, S. Zhang, Y. Wang, L. Yan, *ACS Appl. Polym. Mater.* **2022**, *4*, 2057.
[32] Z. Liu, H. Cheng, H. He, J. Li, J. Ouyang, *Adv. Funct. Mater.* **2022**, *32*, 2109772.
[33] E. Otsuka, A. Suzuki, *J. Appl. Polym. Sci.* **2009**, *114*, 10.
[34] S. Zhang, Y. Zhang, B. Li, P. Zhang, L. Kan, G. Wang, H. Wei, X. Zhang, N. Ma, *ACS Appl. Mater. Interfaces* **2019**, *11*, 32441.
[35] Z. Bai, K. Jia, C. Liu, L. Wang, G. Lin, Y. Huang, S. Liu, X. Liu, *Adv. Funct. Mater.* **2021**, *31*, 2104701.
[36] M. J. Khan, J. Zhang, Q. Guo, *Chem. Eng. J.* **2016**, *301*, 92.
[37] Y. Hou, C. Chen, K. Liu, Y. Tu, L. Zhang, Y. Li, *RSC Adv.* **2015**, *5*, 24023.
[38] P. Yusong, D. Jie, C. Yan, S. Qianqian, *Mater. Technol.* **2016**, *31*, 266.
[39] K. Wang, H. Wang, J. Li, Y. Liang, X.-Q. Xie, J. Liu, C. Gu, Y. Zhang, G. Zhang, C.-S. Liu, *Mater. Horiz.* **2021**, *8*, 2520.
[40] H. Qin, R. E. Owyeung, S. R. Sonkusale, M. J. Panzer, *J. Mater. Chem. C* **2019**, *7*, 601.
[41] C.-W. Lai, S.-S. Yu, *ACS Appl. Mater. Interfaces* **2020**, *12*, 34235.
[42] M. X. Wang, P. Y. Zhang, M. Shamsi, J. L. Thelen, W. Qian, V. K. Truong, J. Ma, J. Hu, M. D. Dickey, *Nat. Mater.* **2022**, *21*, 359.
[43] W. Li, L. Li, S. Zheng, Z. Liu, X. Zou, Z. Sun, J. Guo, F. Yan, *Adv. Mater.* **2022**, *34*, 2203049.
[44] B. Yiming, X. Guo, N. Ali, N. Zhang, X. Zhang, Z. Han, Y. Lu, Z. Wu, X. Fan, Z. Jia, S. Qu, *Adv. Funct. Mater.* **2021**, *31*, 2102773.
[45] K. G. Cho, S. An, D. H. Cho, J. H. Kim, J. Nam, M. Kim, K. H. Lee, *Adv. Funct. Mater.* **2021**, *31*, 2102386.
[46] L. Xu, Z. Huang, Z. Deng, Z. Du, T. L. Sun, Z.-H. Guo, K. Yue, *Adv. Mater.* **2021**, *33*, 2105306.
[47] T. L. Sun, T. Kurokawa, S. Kuroda, A. B. Ihsan, T. Akasaki, K. Sato, M. A. Haque, T. Nakajima, J. P. Gong, *Nat. Mater.* **2013**, *12*, 932.
[48] Y. Huang, L. Xiao, J. Zhou, T. Liu, Y. Yan, S. Long, X. Li, *Adv. Funct. Mater.* **2021**, *31*, 2103917.
[49] M. Wang, P. Zhang, M. Shamsi, J. L. Thelen, W. Qian, V. K. Truong, J. Ma, J. Hu, M. D. Dickey, *Nat. Mater.* **2022**, *21*, 359.
[50] S. Wu, M. Hua, Y. Alsaid, Y. Du, Y. Ma, Y. Zhao, C.-Y. Lo, C. Wang, D. Wu, B. Yao, J. Strzalka, H. Zhou, X. Zhu, X. He, *Adv. Mater.* **2021**, *33*, 2007829.
[51] J. Song, S. Chen, L. Sun, Y. Guo, L. Zhang, S. Wang, H. Xuan, Q. Guan, Z. You, *Adv. Mater.* **2020**, *32*, 1906994.
[52] Y. Ye, Y. Zhang, Y. Chen, X. Han, F. Jiang, *Adv. Funct. Mater.* **2020**, *30*, 2003430.
[53] H. Zhang, N. Tang, X. Yu, Z. Guo, Z. Liu, X. Sun, M.-H. Li, J. Hu, *Chem. Eng. J.* **2022**, *430*, 132779.